Silicon electron-nuclear double-resonance study of the NL10 heat-treatment center

H. H. P. Th. Bekman, T. Gregorkiewicz,* and C. A. J. Ammerlaan
Natuurkundig Laboratorium der Universiteit van Amsterdam, Valckenierstraat 65, NL-1018 XE Amsterdam, The Netherlands
(Received 1 August 1988; revised manuscript received 18 October 1988)

^{29}Si electron-nuclear double-resonance (ENDOR) measurements were performed for the Si-NL 10 center. The results were compared with the ^{29}Si ENDOR measurements of the Si-NL8 spectrum and were found to be similar with the defect electron being even more delocalized in the case of the Si-NL10 center. The wave function is found to be approximately [100] axially symmetric with no symmetry-forbidden mirror planes. This indicates the A_1 ground state for the Si-NL10 defect in analogy with the ground state for Si-NL8. Field-stepped ENDOR measurements show that the ^{29}Si hyperfine interactions originate from a series of different but otherwise very similar centers, each of which generates its own EPR spectrum, which, however, remains unresolved in the EPR experiment. This confirms the results obtained previously from ^{27}Al and ^{17}O ENDOR studies for the Si-NL10 center. The close analogy of the silicon ENDOR data for the Si-NL8 and Si-NL10 centers is indicative of a very similar structure of both centers.

I. INTRODUCTION

Heat treatment of oxygen-rich silicon at about 450 °C leads to the formation of shallow donor states, called thermal donors.[1–3] The first publication on thermal donors appeared in 1954 and during the past three to four decades a tremendous amount of data was gathered on the subject—for a review see, e.g., Bourret.[4] It is nowadays established that upon heat treatment in the 300–500 °C region a series of very similar shallow double-donor centers is created.[5] They can be observed by standard infrared techniques and up to nine different species have been reported.[6]

The formation of thermal donors (as monitored in infrared) is accompanied by the simultaneous generation of the electron-paramagnetic-resonance (EPR) spectra. The EPR studies revealed the creation of centers with predominantly $2mm$ point-group symmetry.[7,8] Further studies showed that the Si-NL8 and Si-NL10 spectra were practically the only ones which could be related to the thermal-donor (TD) centers as observed in infrared. For one of these—the Si-NL8 spectrum—a direct identification with the singly ionized state of the infrared double donors was made.[9] At the same time the role of the Si-NL10 center whose concentration was well correlated to the thermal-donor concentration in all types of material (p or n type)[10,11] remained unclear.

The involvement of oxygen in the growth of thermal donors was generally assumed, almost since their discovery in 1954. However, only recently, after a successful diffusion of the oxygen-17 isotope, the oxygen incorporation could be established for the Si-NL10 center.[12] Later, a similar result has been obtained also for the Si-NL8 center.[13]

The microscopic structure of the thermal donors has been investigated by means of the electron-nuclear double-resonance (ENDOR) technique.[13–15] For the Si-NL8 center the ^{29}Si-ENDOR data are currently available.[14] Quite recently also preliminary results of the ^{17}O-ENDOR experiment have been reported for that center.[13] For the Si-NL10 spectrum an extensive ENDOR study has been performed.[15] A floating-zone (FZ) aluminum-doped sample diffused with oxygen-17 was used. The hyperfine interactions were measured with the oxygen and aluminum nuclei as both impurities were found to be incorporated in the structure of the center. Also the quadrupole interactions with these impurities, which both have nuclear spin $I=\frac{5}{2}$, were analyzed. On the basis of the results a detailed microscopic model of the Si-NL10 center was proposed. According to the model a series of similar centers is formed, the smallest species involving two oxygen atoms. It grows by addition of a single oxygen atom at a time. The oxygen atom takes then the normal bond-centered position in one of the mirror planes of the defect. The aluminum ENDOR study showed that a single aluminum atom was present in the center regardless of its growth stage. It appeared however, that aluminum was not really necessary in the formation of the Si-NL10 center. Due to its affinity to oxygen it takes, when present, an active part in the oxygen aggregation. The core of the center involves a vacancy which is created to release the stress built up during the oxygen aggregation.

The experiment reported in this paper gives ENDOR data on hyperfine interactions with silicon-29 nuclei, thus completing the ENDOR data for the Si-NL10 heat-treatment center.

II. EXPERIMENTAL PROCEDURE

A. Equipment

The measurements were performed with a superheterodyne spectrometer operating at 23 GHz and adjusted to detect the dispersion part of the EPR signal. The magnetic field, modulated at a frequency of 83 Hz, could be rotated in the $(0\bar{1}1)$ plane of the sample. A cylindrical TE_{011}-mode silver-coated Epibond cavity was used. In

 ©1989 The American Physical Society

the thin silver layer on the cylindrical side wall of the cavity a spiral groove was cut which could serve as an ENDOR coil. For ENDOR measurements the radio frequency was square-wave modulated at 3.3 Hz to allow double phase-sensitive detection of the signal. The sample was held at 4.2 K. The ENDOR measurements were performed under white light illumination. Light from a halogen source was transmitted to the sample by a quartz rod.

B. The sample

The sample used for the experiment was commercial (Wacker Chemitronic) aluminum-doped, FZ silicon with a resistivity $\rho \sim 2$ Ω cm, aluminum concentration $[\mathrm{Al}]=9\times10^{15}$ cm^{-3} and carbon concentration less than 5×10^{15} cm^{-3}. It had dimensions of $2\times2\times15$ mm^3 with its longest side corresponding to the $[0\bar{1}1]$ direction. The sample was further diffused with oxygen in the ultraclean diffusion procedure as described previously.[10] The total oxygen concentration, measured by the infrared absorption in the 9-μm band was 4×10^{17} cm^{-3}, 30% of it being the ^{17}O magnetic isotope. After the diffusion process, the sample was heated up to 1380 °C for $\frac{1}{2}$ h. This was followed by a rapid quench to room temperature. Finally the sample was given a heat treatment for 200 h at 470 °C. After the 200-h anneal the sample was on the brink of *p*- to *n*-type conversion. The EPR spectrum showed a strong Si-NL10 signal with a concentration of EPR-active centers of $\sim10^{16}$ cm^{-3}. The same sample has previously been used for ^{17}O and ^{27}Al ENDOR measurements whose results were published in advance.[15]

III. EXPERIMENTAL RESULTS

A. General

1. Spin Hamiltonian

The Si-NL10 EPR spectrum can be described with the simple spin Hamiltonian

$$\mathcal{H}=\mu_B \mathbf{B}\cdot\overleftrightarrow{g}\cdot\mathbf{S}\ , \tag{1}$$

with spin $\mathbf{S}=\frac{1}{2}$. The symmetry of the defect wave function is reflected directly by the symmetry of the *g* tensor which in this case is orthorhombic, with point group $2mm$. There are six different orientations possible in the silicon lattice for such a defect. These have been labeled here *ab*, *ac*, *ad*, *bc*, *bd*, and *cd* following the convention used by Sprenger *et al.* for the V^- center.[16] Because the rotation of the magnetic field takes place in the $(0\bar{1}1)$ plane, at most four different EPR lines can be observed in the experiment. The characteristic angular dependence of the Si-NL10 spectrum (in one of its later transformation stages) labeled with the corresponding orientations is shown in Fig. 1. The principal values for the *g* tensor are $g_1=1.997\,99$, $g_2=1.999\,46$, and $g_3=1.999\,82$. Wherever orientation dependent information is given in this paper we will refer to the orientation labeled *ad*. In Fig. 2 the cubic axes system x,y,z is depicted for defect orientation

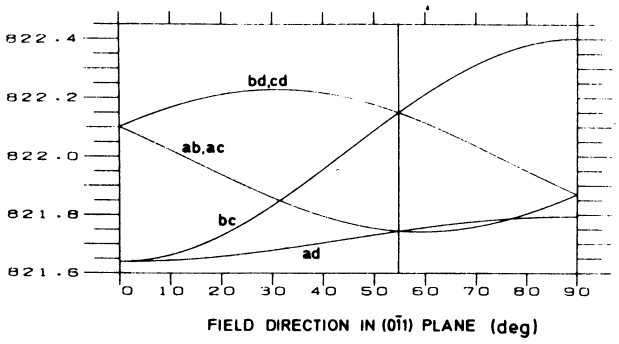

FIG. 1. The angular dependence of the Si-NL10 EPR spectrum, microwave frequency 23 GHz. The orientations are labeled in accordance with Sprenger *et al.* (Ref. 16).

ad. Also the principal axes of the *g* tensor are shown. For this orientation the [100] direction is the twofold axis, the $(0\bar{1}1)$ and the (011) crystallographic planes constitute the two mirror planes of the defect.

When the interaction with only one magnetic nucleus (with spin **I**) is added, then one can generally expect that the symmetry is lowered. The Hamiltonian can then be written as

$$\mathcal{H}=\mu_B \mathbf{B}\cdot\overleftrightarrow{g}\cdot\mathbf{S}-g_N\mu_N\mathbf{B}\cdot\mathbf{I}+\mathbf{S}\cdot\overleftrightarrow{A}\cdot\mathbf{I}\ . \tag{2}$$

The symmetry of the center together with the magnetic nucleus is now reflected in the symmetry of the *A* tensor. In the most general case the magnetic nucleus takes a position somewhere around the defect and not on one of the two mirror planes. The resulting symmetry is then triclinic and yields a triclinic *A* tensor of general class (*G* class). When the magnetic nucleus is lying on one of the mirror planes the resulting symmetry is monoclinic, point

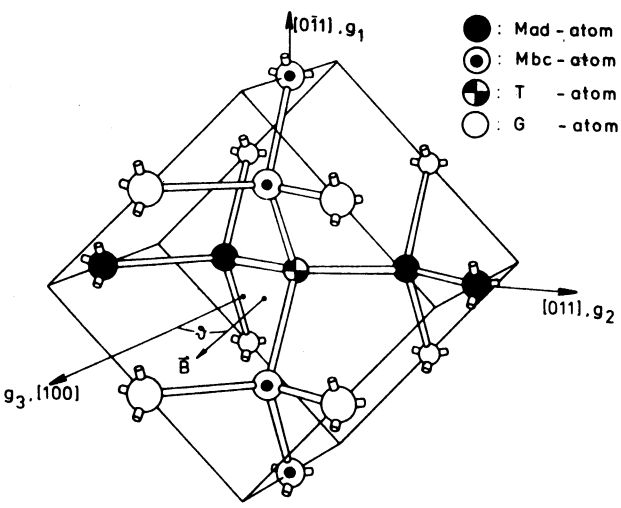

FIG. 2. The silicon lattice with the cubic axis system as used in the tables of the hyperfine tensors. Also the principal directions of the *g* tensor for defect orientation *ad* are depicted, and the different types of atoms as can be discriminated in the experiment.

group m (M class). Since the two mirror planes are not equivalent it is possible in the experiment to distinguish them; as a result two classes of interaction (*Mad* and *Mbc* class) may be observed experimentally. Finally there is the possibility that the magnetic nucleus is lying on the twofold axis, which results in a $2mm$ point-group symmetry for the A tensor (T class). The above is summarized in Table I and in Fig. 2, where the different positions of the interacting nuclei are indicated.

From the Hamiltonian in Eq. (2) first-order solutions can be written down

$$E_{|m_S,m_I\rangle}=m_S g_{\text{eff}}\mu_B B-m_I g_N\mu_N B+m_S m_I A_{\text{eff}} . \tag{3}$$

NMR transitions are determined by $\Delta m_S=0$, $\Delta m_I=\pm 1$. For a nuclear spin of $\mathbf{I}=\frac{1}{2}$ the NMR (and ENDOR) frequencies are

$$h\nu=\Delta E=|g_N\mu_N B+\tfrac{1}{2}A_{\text{eff}}| , \tag{4a}$$

$$h\nu=\Delta E=|g_N\mu_N B-\tfrac{1}{2}A_{\text{eff}}| . \tag{4b}$$

EPR transitions are determined by $\Delta m_S=\pm 1$, $\Delta m_I=0$. For a spin of $\mathbf{S}=\frac{1}{2}$ the first-order solutions are

$$h\nu=\Delta E=g_{\text{eff}}\mu_B B+\tfrac{1}{2}A_{\text{eff}} , \tag{5a}$$

$$h\nu=\Delta E=g_{\text{eff}}\mu_B B-\tfrac{1}{2}A_{\text{eff}} . \tag{5b}$$

In the analysis of the experimental results the parameters of the spin Hamiltonian as given by Eq. (2) were fitted with help of a Control Data Corporation Cyber-170 model-750 mainframe computer. The basic routines used were obtained from the International Mathematical and Statistical Library. The routines allowed also the simulation of the ENDOR spectra.

2. *Linear-combination-of-atomic-orbitals (LCAO) analysis*

The interaction between the electronic spin $\mathbf{S}$ and the nuclear spin $\mathbf{I}$ can be represented quantum mechanically by a dipole-dipole interaction operator. The hyperfine interaction tensor follows from integration of this operator over the spatial part of the electronic wave function. The hyperfine tensor can be decomposed into an isotropic and a traceless part

$$\overleftrightarrow{A}=a\overleftrightarrow{1}+\overleftrightarrow{B} . \tag{6}$$

The isotropic part is the Fermi-contact interaction which is proportional to the density of the electronic wave function at the site r_0 of the nucleus:

$$a=\tfrac{2}{3}\mu_0 g_{\text{eff}}\mu_B g_N\mu_N|\Psi(r_0)|^2 , \tag{7}$$

where Ψ is the electronic wave function. The anisotropic tensor $\overleftrightarrow{B}$ describes the classical dipole-dipole interaction and can be written

$$B_{ij}=\frac{\mu_0}{4\pi}g_{\text{eff}}\mu_B g_N\mu_N\left\langle\Psi\left|\frac{3x_ix_j}{r^5}-\frac{\delta_{ij}}{r^3}\right|\Psi\right\rangle , \tag{8}$$

where $x_i,x_j=x,y,z$.

Electronic wave functions of defects in silicon are often described as linear combinations of atomic orbitals (LCAO). A one-electron wave function is then written as

$$\Psi=\sum_i \eta_i\phi_i , \tag{9}$$

where i enumerates lattice sites and the contributions ϕ_i on these sites are hybrid combinations of silicon $3s$ and $3p$ orbitals:

$$\phi_i(\mathbf{r})=\alpha_i\psi_s(\mathbf{r})+\beta_i\psi_p(\mathbf{r}) . \tag{10}$$

Substitution of Eqs. (9) and (10) into Eqs. (7) and (8) yields for the Fermi-contact interaction

$$a_i=\tfrac{2}{3}\mu_0 g_{\text{eff}}\mu_B g_N\mu_N\eta_i^2\alpha_i^2|\psi_s(0)|^2 \tag{11}$$

under the assumption that ψ_s and ψ_p decrease sufficiently fast with the distance $\mathbf{r}$, that at site i only the contribution from orbitals centered on atom i itself has to be taken into account. Similarly, the anisotropic interaction gives an axial hyperfine tensor $\overleftrightarrow{B}_i$ with principal values $(2b_i, -b_i, -b_i)$, whose axial direction is the direction of the p lobe and where b_i has the value

$$b_i=\frac{\mu_0}{4\pi}g_{\text{eff}}\mu_B g_N\mu_N\eta_i^2\beta_i^2\tfrac{2}{5}\langle r^{-3}\rangle_p . \tag{12}$$

The quantities $|\psi_s(0)|^2$ and $\langle r^{-3}\rangle_p=\langle\psi_p|r^{-3}|\psi_p\rangle$ are taken as constants from the atomic wave functions and independent of the specific defect or molecule. When they are known, then with the normalization $\alpha_i^2+\beta_i^2=1$ the s-character fraction α_i^2, the p-character fraction β_i^2, and the degree of localization η_i^2 of the paramagnetic electron on the atomic site i can be determined. In the analysis of our ENDOR results we will use $|\psi_s(0)|^2=34.6\times 10^{30}\ \text{m}^{-3}$ and $\langle r^{-3}\rangle_p=18.2\times 10^{30}\ \text{m}^{-3}$ as given by Morton and Preston.[17] It is clear that, because of the axial character of the p orbitals this analysis

TABLE I. Properties of the different types of hyperfine tensors and associated shells for a spectrum of $2mm$ point-group symmetry like the Si-NL10. N_{at} is the number of atoms per shell and N_{el} is the number of independent tensor elements. The number of ENDOR lines is indicated for the three high-symmetry directions in the $(0\bar{1}1)$ plane.

Class	Symmetry	N_{el}	N_{at}	Atom positions	No. of lines $\mathbf{B}\parallel[100]$	$\mathbf{B}\parallel[111]$	$\mathbf{B}\parallel[011]$
T	$2mm$	3	1	[100] axis	2	2	3
Mad	m	4	2	$(0\bar{1}1)$ plane	2	3	4
Mbc	m	4	2	(011) plane	2	3	4
G	1	6	4	others	3	4	6

is only fully valid in the case of axial hyperfine tensors. Moreover, a_i and b_i must have the same sign. All the fitted tensors obey the latter condition.

The experimentally observed hyperfine interactions are not always exactly axial. They can be expressed by so-called reduced parameters by equating the principal values to $a+2b$, $a-b+c$, and $a-b-c$, where a is the isotropic part, b is the parameter determining the axially symmetric part, and c is the deviation from axial symmetry. The parameters b and c are chosen such that $|b|>|c|$.

For deep centers with missing or dangling bonds the LCAO analysis is successful. The total localization adds up to values close to 100%. Sometimes localizations over 100% are found, which is due to effects not accounted for in the LCAO treatment, e.g., core polarization. However, for the shallow donors like P, As, and Sb the LCAO analysis turns out to be less applicable. In our experiment the biggest hyperfine interaction is found to have an isotropic part $a=2.51$ MHz. This corresponds to a localization of 0.07%. In this way the LCAO analysis confirms that we are dealing with a very shallow defect. A comparison with the silicon ENDOR results for the Si-NL8 spectrum obtained by Michel *et al.*[14] shows that the wave function of the Si-NL10 defect is more delocalized. In case of the Si-NL8 spectrum the biggest hyperfine interaction has an isotropic a value of 9.89 MHz, which gives a localization of 0.277%.

B. Silicon-29 ENDOR

Natural silicon contains three isotopes, ^{28}Si, ^{29}Si, and ^{30}Si. Only the ^{29}Si isotope with its natural abundance of 4.7% has a nonzero nuclear spin of $I=\frac{1}{2}$.

In our experiment the Zeeman frequency ($=g_N\mu_N B/h$) for the ^{29}Si nucleus was around 7.0 MHz.

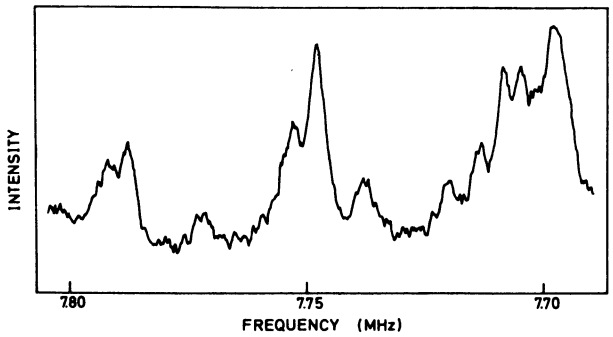

FIG. 3. Part of the original ENDOR spectrum close to the crowded Zeeman valley. The ENDOR pattern originates from a single EPR orientation and the magnetic field is in the $(0\bar{1}1)$ plane.

In the [100] direction, the ENDOR lines appeared in the frequency range from 5.7 to 8.3 MHz. In this region the ^{17}O-ENDOR and the ^{27}Al-ENDOR lines are not interfering. In the [100] direction we have looked for silicon ENDOR up to 18.75 MHz. Silicon ENDOR lines above 18.75 MHz are unlikely, because those lines would show in the EPR experiment. The biggest interaction observed was near 8.3 MHz, corresponding to an isotropic hyperfine interaction of about 2.5 MHz. The full width at half maximum linewidth of the ^{29}Si ENDOR was 5–8 kHz (i.e., significantly more than for the ^{17}O ENDOR lines). Part of the original ENDOR spectrum is shown in Fig. 3, for the magnetic field somewhere in the $(0\bar{1}1)$ plane. The high resolution obtained in the experiment is nicely demonstrated.

From the measurements only the biggest hyperfine interactions could be analyzed; the interactions at lower frequency were severely overlapping. Six hyperfine ten-

TABLE II. Hyperfine parameters for the six fitted silicon tensors. The tensors are given in the standard orientation *ad*, the tensor components and the principal values are in kHz. Each principal value is followed by a normalized principal direction.

Shell	$\overleftrightarrow{A}$			i	A_i	$\mathbf{n}_i$
Si-*T*1	2545.7	0.0	0.0	1	2545.7	(1.00, 0.00, 0.00)
	0.0	2488.2	2.2	2	2490.4	(0.00, 0.71, 0.71)
	0.0	2.2	2488.2	3	2486.0	(0.00, −0.71, 0.71)
Si-*T*2	2505.8	0.0	0.0	1	2505.8	(1.00, 0.00, 0.00)
	0.0	2430.5	−1.0	2	2431.6	(0.00, −0.71, 0.71)
	0.0	−1.0	2430.5	3	2429.5	(0.00, 0.71, 0.71)
Si-*T*3	2475.1	0.0	0.0	1	2475.1	(1.00, 0.00, 0.00)
	0.0	2418.1	−2.7	2	2420.8	(0.00, −0.71, 0.71)
	0.0	−2.7	2418.1	3	2415.5	(0.00, 0.71, 0.71)
Si-*G*1	2016.2	0.0	0.0	1	2016.2	(1.00, 0.00, 0.00)
	0.0	1993.3	0.0	2	1993.3	(0.00, 1.00, 0.00)
	0.0	0.0	1979.2	3	1979.2	(0.00, 0.00, 1.00)
Si-*G*2	1907.5	0.1	−0.1	1	1907.5	(1.00, 0.00, −0.00)
	0.1	1858.3	0.3	2	1874.9	(0.00, 0.02, 1.00)
	−0.1	0.3	1874.9	3	1858.3	(0.00, −1.00, 0.02)
Si-*G*3	1817.2	0.1	−0.2	1	1817.2	(1.00, 0.00, −0.00)
	0.1	1770.2	0.1	2	1782.3	(0.00, 0.01, 1.00)
	−0.2	0.1	1782.3	3	1770.2	(0.00, 1.00, 0.01)

TABLE III. Reduced tensor parameters of the silicon hyperfine interactions in kHz, also the percentages of s and p character, α^2 and β^2 respectively, and the localizations η^2 per atom are given.

Shell	a	b	c	a/b	b/c	α^2 (%)	β^2 (%)	η^2 (%)
Si-$T1$	2507.4	19.2	2.2	130.6	8.7	76	24	0.07
Si-$T2$	2455.6	25.1	1.0	97.8	24.4	71	29	0.08
Si-$T3$	2437.1	19.0	2.7	128.3	7.2	76	24	0.07
Si-$G1$	1996.2	10.0	7.0	199.4	1.4	83	17	0.05
Si-$G2$	1880.3	13.6	8.3	137.8	1.6	77	23	0.05
Si-$G3$	1789.9	13.7	6.0	131.1	2.3	77	23	0.05

sors were fitted. The fits were made with $g_N\mu_N/h = 8.459$ MHz T^{-1}, i.e., $g_N = 1.1097$ as experimentally determined by Sprenger *et al.*,[16] which deviates slightly from the value found in literature. The deviation between the experimental points and the fit was never more than 2 kHz, which is well within the linewidth.

By inspection of the results of the computer fits it is apparent that all the hyperfine tensors, which are otherwise almost isotropic, exhibit some [100] axiality. The absolute sign of a tensor cannot be determined from the ENDOR measurements. Therefore for all hyperfine tensors the isotropic part, $a = \frac{1}{3}\mathrm{Tr}(\overleftrightarrow{A})$, is given as a positive value. Subsequently, the tensors that could be fitted are ordered with decreasing a values. The experimental results are given in Table II. The tensors are shown in standard orientation *ad*. The LCAO parameters are given in Table III.

C. Field-stepped ENDOR

The field-stepped ENDOR (FSt ENDOR) technique relates directly the ENDOR transition with the EPR line of its origin. As a result the high resolving power of ENDOR is used to unravel the structure of the EPR spectrum. The level scheme in case of $S=\frac{1}{2}$ and $I=\frac{1}{2}$ is shown in Fig. 4. The allowed EPR and NMR transitions are indicated. As can be seen, ENDOR transition $1\leftrightarrow 2$ and $3\leftrightarrow 4$ can be observed on either of the two EPR transitions. If the $1\leftrightarrow 2$ ENDOR transition is monitored for different magnetic field values then the intensity of the ENDOR line should exhibit two maxima for magnetic field values corresponding to the $1\leftrightarrow 3$ and $2\leftrightarrow 4$ EPR transitions. The two EPR transitions are separated by the hyperfine interaction constant A_{eff}. For small values of A_{eff} the two field-stepped ENDOR peaks overlap, resulting in one broad peak with its width proportional to the hyperfine constant A_{eff}. This corresponds well with the situation depicted in Fig. 5.

The results of the FSt ENDOR experiment confirm the conclusion from the oxygen and aluminum ENDOR (Ref. 15) that the EPR spectrum is a superposition of different species, as illustrated in Fig. 5. It can be seen that the two lines which correspond to different tensors attain their maximum for different field values. Due to the required signal-to-noise ratio the FSt ENDOR experiment can only be performed for ENDOR lines of relatively high intensity. No systematic study was made for the fitted hyperfine tensors. The experience from the previous oxygen and aluminum FSt ENDOR studies indicates that the three $2mm$ (T-class) tensors probably originate from three different EPR species, with localizations on individual atoms decreasing for later species. In the EPR experiment not only the hyperfine interaction with ^{29}Si atoms, but also the different species are unresolved. It has been noted that the Si-NL8 and Si-NL10 spectra exhibit so called "g shifting" upon prolonged annealing at 450 °C.[8,10,18] This effect for Si-NL10 can now easily be explained; different Si-NL10 species have slightly

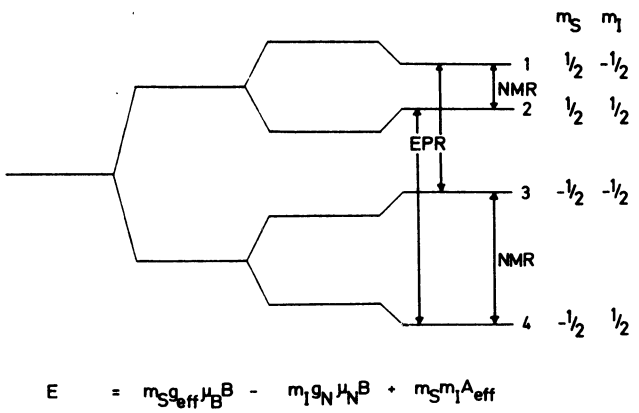

FIG. 4. Schematic representation of the energy-level scheme for the system with electron spin $S=\frac{1}{2}$ and nuclear spin $I=\frac{1}{2}$. The allowed EPR and NMR transitions are indicated.

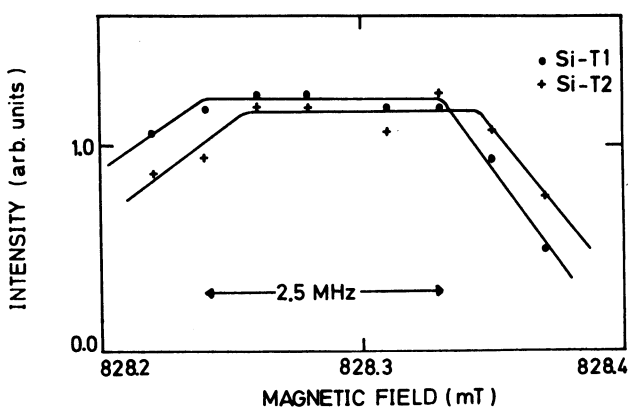

FIG. 5. The illustration of the field-stepped ENDOR technique as applied to reveal the different species in the EPR spectrum. The intensity of two ENDOR tensors is depicted as a function of the magnetic field position. The magnetic field is in the $(0\bar{1}1)$ plane.

different g values and a varying concentration of different species can result in a semicontinuous g-shifting process. A similar mechanism is most probably responsible also for the g shifting of the Si-NL8 spectrum.

IV. DISCUSSION

A. Shallow-center character of Si-NL10

One of the characteristic features of shallow centers is a low total localization traced in the experiment. The LCAO treatment works well with localized deep defects, as already pointed out in Sec. III A 2. A deep defect produces a ground-state wave function with big gradients over the ligand atoms. In the LCAO analysis the wave function at the ligands can be approximated by a linear combination of $3s$ and $3p$ silicon atomic orbitals, centered on that ligand. For a deep defect the wave function can quite often be approximated by almost one sp^3-hybridized orbital. This results in a hyperfine tensor being approximately axial along a $\langle 111 \rangle$ bonding direction. For an electron in an orbital pointing in any of the four $\langle 111 \rangle$ directions an sp^3-hybridized orbital with $\alpha^2 = 25\%$ is expected. Most of the hyperfine tensors of deep defects are $\langle 111 \rangle$-axially symmetric and it is apparent that the p character is then stronger—e.g., $\alpha^2 = 16.5\%$ on average for the axial tensors of VV^-.[19]

For a shallow defect all four sp^3-hybridized bonds contribute. If the four sp^3 bonds are equally occupied the hyperfine tensor is isotropic and in the LCAO analysis we will find only an s contribution. For a shallow defect we will observe therefore mainly the s part of the wave function, i.e., $\alpha^2 > 0.25$, or $\beta^2/\alpha^2 \ll 3$, and most of the p contribution cancels (big a/b ratio). This results in the underestimation of the localization $\eta^2, \eta^2_{\text{total}} \ll 100\%$. Therefore, a shallow defect is characterized by

$$(1)\, \eta^2_{\text{total}} \ll 100\% \ ,$$

$$(2)\, \frac{\beta^2}{\alpha^2} \ll 3 \ .$$

Equations (11) and (12) give $a/b = (20\pi/3)|\psi_s(0)|^2\alpha^2/(\langle r^{-3} \rangle \beta^2)$, therefore criterion 2 can be replaced by $a/b \gg 13$. All three criteria are shown in Tables IV(a) and IV(b), for a few tensors of two typical deep centers V^-, VV^- and two typical shallow donor centers P,As. In Table IV(c) the corresponding values are shown for heat-treatment centers Si-NL10 and Si-NL8. As can be seen, both heat-treatment centers clearly fall in the class of shallow effective-mass centers.

The shallow character of the center can also be deduced from the g value. The g value or g tensor of the defect is an important EPR parameter; it acts as a characteristic identification mark to distinguish between all the different EPR centers. Unfortunately theoretical interpretation of the g tensor is a very complicated problem. Even for relatively simple cases as the shallow donor and acceptor impurities, whose wave functions are known in sufficient detail no satisfactory calculations of g values are available.[20–23] For the more complicated systems of lattice defects in silicon, generally of deep level character, at most qualitative considerations can be given. On the other hand Lee and Corbett[24] proposed an empirical classification of g values, which has further been extended by Sieverts.[25] In this classification scheme four different types of defects are distinguished. Type A, vacancy-type defects with one dangling bond or two parallel dangling bonds; type B, vacancy-type defects with two or more dangling bonds under tetrahedral angles; type C, interstitialcies; type D, impurities on substitutional and interstitial sites.

In the proposed scheme g values of defect centers are represented in a two-dimensional plot of reduced g values. The reduced g values are constructed from the principal g values by assuming them to be axially symmetric. Then the most deviating g value is defined as the parallel value $g_{\parallel}$ and the average of the other two principal g values is the perpendicular value $g_{\perp}$. If then $g_{\parallel}$ is plotted against $g_{\perp}$ different types of defects will group in different sections of the diagram. In Fig. 6 the small section of the diagram grouping shallow defects and impurities of type D is shown. As can be seen the heat-treatment centers Si-NL8 and Si-NL10-13-17 (presently identified to be one center) both have their g values in this particular region.

B. Symmetry of ground-state wave function

Wave functions of shallow centers can be described with the effective-mass theory of Kohn and Luttinger.[26,27] The wave function of a donor electron in its

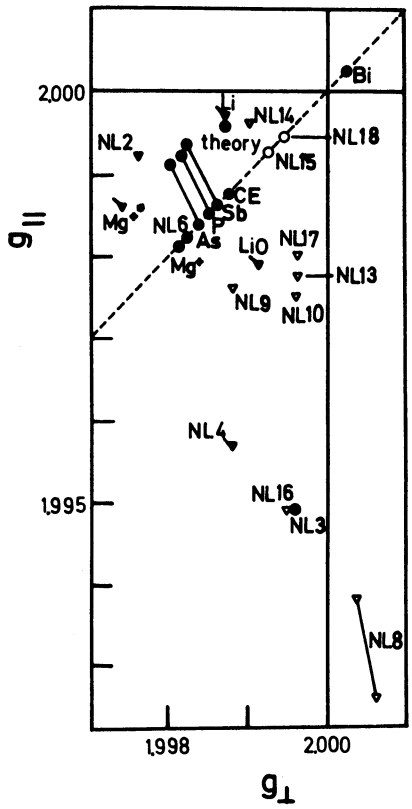

FIG. 6. Plot of g values of shallow or effective-mass donor impurities and defects, after Sieverts (Ref. 25).

TABLE IV. Hyperfine parameters in kHz for (a) some typical ⟨111⟩ axial silicon hyperfine tensors of two characteristic deep defects V^- and VV^- after Sprenger *et al.* (Ref. 16) and Sieverts *et al.* (Ref. 19). (b) Some typical silicon hyperfine tensors of two characteristic shallow defects phosphorus and arsenic on substitutional positions after Hale and Mieher (Ref. 31). (c) Two prominent silicon interactions for the Si-NL8 and Si-NL10 spectrum after Michel *et al.* (Ref. 14) and Table III. Only one species is concerned.

(a)

Center	η^2_{total}	Tensor	a	b	c	a/b	β^2/α^2	η^2 (%)
V^-	114.76%	*G*1	13 366.0	2039.3	64.4	6.55	6.14	2.08
		*G*26	239.3	36.7	4.0	6.53	6.14	0.04
		*Mad*1	355 845.6	22 303.4	1262.9	15.95	2.52	27.28
		*Mad*17	203.7	23.1	1.5	8.80	4.56	0.02
VV^-	118.90%	*G*1	31 470	2230	460	14.11	2.91	2.97
		*G*20	297	59	3	5.03	8.09	0.07
		*M*1	195 200	23 300	100	8.38	4.88	27.71
		*M*12	701	97	2	7.23	5.67	0.11

(b)

Center	η^2_{total}	Tensor	a	b	c	a/b	β^2/α^2	η^2 (%)
P_{subst}	14.58%	*B*	4508	70.6	18.6	63.9	0.631	0.160
		C	3298	5.0	0.0	659.6	0.060	0.076
		I	1370	21.4	2.2	64.0	0.629	0.049
		R	758	18.4	7.6	41.2	0.976	0.033
As_{subst}	18.86%	*B*	6000	105.2	22.2	57.0	0.706	0.223
		C	4074	5.8	0.0	702.4	0.057	0.094
		I	1436	23.1	1.3	62.2	0.647	0.051
		R	856	23.1	10.7	37.1	1.088	0.039

(c)

Center	η^2_{total}	Tensor	a	b	c	a/b	β^2/α^2	η^2 (%)
Si-NL8	5.64%	1	9890	70	−30	141.3	0.285	0.277
		2*a*	8530	60	−30	142.2	0.284	0.221
Si-NL10	0.28%	Si-*T*1	2507.4	19.2	2.2	130.6	0.316	0.071
		Si-*G*1	1996.2	10.0	7.0	199.4	0.202	0.052

ground state can be approximately represented by a linear combination of six wave functions corresponding to the six minima of the conduction band which for silicon lie along the ⟨100⟩ directions. The wave function has the form

$$\Psi(\mathbf{r})=\left[\frac{1}{\sum_j \alpha_j^2}\right]^{1/2}\sum_{j=1}^{6}\alpha_j F^{(j)}(\mathbf{r})u^{(j)}(\mathbf{r})\exp(i\mathbf{k}_0^j\cdot\mathbf{r}) , \tag{13}$$

where j refers to the different minima, $u^{(j)}(\mathbf{r})\exp(i\mathbf{k}_0^j\cdot\mathbf{r})$ is the Bloch wave at the jth minimum, and $F^{(j)}(\mathbf{r})$ is a hydrogenlike envelope function. Table V gives the combinations of one-minimum wave functions which are allowed in the case of $2mm$ point-group symmetry. The wave functions of types A_2, B_1, and B_2 are zero on one or two of the mirror planes. The probability density of the electron on atoms which are situated in those "forbidden" mirror planes would not only be low because of the widely spread character of the shallow donor wave function, but even zero by the symmetry.

The biggest hyperfine interaction found in the present ENDOR experiment has $2mm$ point-group symmetry indicating that none of the two mirror planes is symmetry forbidden. Therefore the ground-state wave function of the Si-NL10 defect has A_1 symmetry. As can be seen from Table V, three possible combinations of the six conduction-band minima are then possible.

Inspection of Table II shows that all the observed hyperfine tensors have an approximate [100] axial character. The tensors in Table II are given in standard orientation *ad*, with the twofold axis along [100]. The axial direction of the tensors coincides therefore with the twofold axis of the defect. However, this feature of the

TABLE V. Symmetry allowed combinations of wave functions of conduction-band minima in $2mm$ point-group symmetry. The twofold axis is along x.

Wave-function symmetry	Coefficients for conduction-band valleys x	$-x$	y	$-y$	z	$-z$
A_1	0	0	1	1	1	1
A_1	0	1	0	0	0	0
A_1	1	0	0	0	0	0
A_2	0	0	1	1	−1	−1
B_1	0	0	1	−1	−1	1
B_2	0	0	1	−1	1	−1

ground-state wave function offers no extra information to discriminate between the three available A_1 states; as can be seen in Table V all three of them allow the [100] axiality.

The results of the ^{29}Si-ENDOR study of the Si-NL8 center[14] appear very similar. The biggest localization is observed for atoms on the twofold axis, while most of the tensors show near [100] axiality. Therefore the ground-state wave function of the Si-NL8 defect also has A_1 symmetry. In case of the Si-NL8 defect additional information is available from infrared (ir) measurements under uniaxial stress. Stavola and Lee[28] concluded from the stress response of the ir that the ground state of the thermal donor (Si-NL8 spectrum is related to the TD$^+$ level[9]) is constructed from a single pair of conduction-band valleys along the x axis. From the wave functions consistent with the $2mm$ point-group symmetry of the defect only two of the A_1 symmetry type can be constructed in this way.

In the case of the Si-NL10 center, despite its large concentrations, no identification with ir levels has been made. Therefore no additional information is available about the ground-state wave function and three A_1 symmetry combinations are possible.

C. Si-NL8 and Si-NL10 hyperfine tensors

In Figs. 7 and 8 the angular dependence of the $\overleftrightarrow{A}$ tensor is depicted for the first two shells within one species for both Si-NL8 and Si-NL10. Figures 7(a) and 8(a) show the orthorhombic $\overleftrightarrow{A}$ tensors of $2mm$ point-group symmetry. Figures 7(b) and 8(b) show a triclinic, point-group 1 tensor. (Within the available resolution of the linewidth the tensor appears as orthorhombic II which is, however, not allowed for orthorhombic-I, point-group $2mm$ symmetry.)

The hyperfine interactions of the Si-NL8 and Si-NL10 look alike. This is best illustrated by Figs. 7(b) and 8(b). The angular dependences of these two triclinic tensors match perfectly, if the numbers on the vertical axis are ignored. Also the tensors depicted in Figs. 7(a) and 8(a) are similar, with slightly bigger anisotropy of the latter one. It seems that the Si-NL8 and Si-NL10 defect structures are very similar, with the Si-NL10 defect originating from a more shallow level than Si-NL8. In case of the Si-NL10 hyperfine tensors of $2mm$ class, the linewidth is too big to observe the small splittings of the

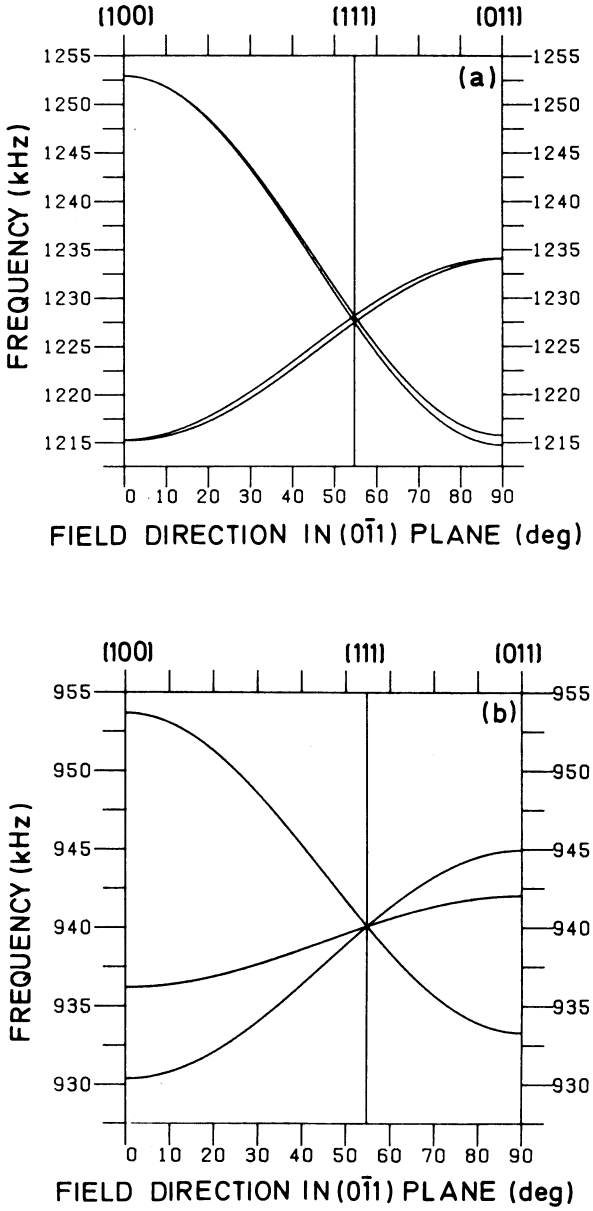

FIG. 7. Computer simulation of the angular dependence of two silicon hyperfine tensors of the Si-NL10 spectrum (a) Si-$T2$ and (b) Si-$G2$. The two tensors belong most probably to one species. $\frac{1}{2}A_{\rm eff}$ is plotted.

TABLE VI. (a) Hyperfine parameters for the $2mm$ tensor fitted as if it was a mirror-class tensor. The tensor is given in the standard orientation ad, and the tensor values and the principal values are in kHz. Each principal value is followed by a normalized principal direction. (b) Reduced tensor parameters of the above silicon hyperfine interaction in kHz, also the percentages of s and p character, α^2 and β^2, respectively, and the localization η^2 are given.

(a)

Shell	$\overleftrightarrow{A}$			i	A_i	$\mathbf{n}_i$
Si-$M1$	2505.8	0.4	−0.4	1	2505.8	(1.00, 0.01, −0.01)
	0.4	2430.6	−1.1	2	2431.7	(0.01, −0.71, 0.71)
	−0.4	−1.1	2430.6	3	2429.6	(0.00, −0.71, 0.71)

(b)

Shell	a	b	c	a/b	b/c	α^2 (%)	β^2 (%)	η^2 (%)
Si-$M1$	2455.7	25.1	1.1	98.0	23.8	71	29	0.08

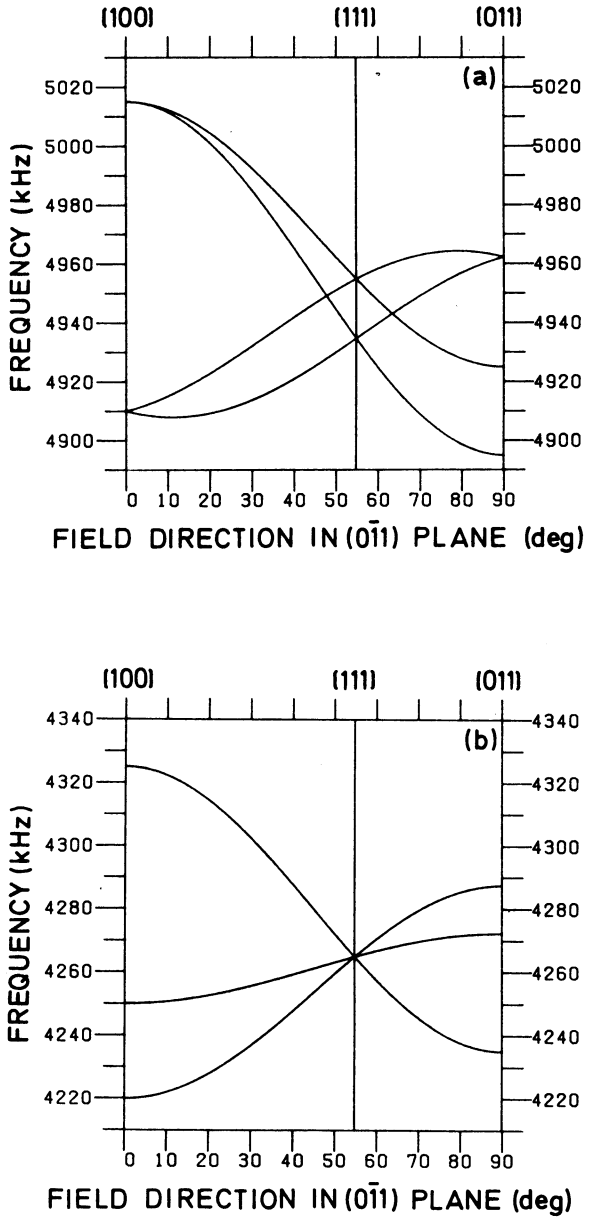

FIG. 8. Computer simulation of the angular dependence of two silicon hyperfine tensors of the Si-NL8 spectrum after Michel *et al.* (Ref. 14) (a) 1 and (b) 2a. The two tensors belong to one species. $\frac{1}{2}A_{\text{eff}}$ is plotted.

closed and open loop. As a result a similar fit to the experimental results can be made assuming lower symmetry of point group m. Such a fit of one of the $2mm$ tensors under assumption of m symmetry has been made. The resulting hyperfine tensor as given in Tables VI(a), and VI(b) and depicted in Fig. 9 is experimentally indistinguishable from the one fitted with the assumed $2mm$ point-group symmetry [as given in Table II (Si-$T2$) and depicted in Fig. 7(a)]. It is common practice to choose the highest possible symmetry which can describe the experimental data. However, one has to be aware of this degree of freedom while constructing a microscopic model.

D. Models for the Si-NL10 center

The ^{29}Si-ENDOR data offers no possibilities to construct a microscopic model for the Si-NL10 center. It can, however, serve to check the validity of the existing models. In this way the Ourmazd-Schröter-Bourret (OSB) -like model,[29] rejected previously for the Si-NL8

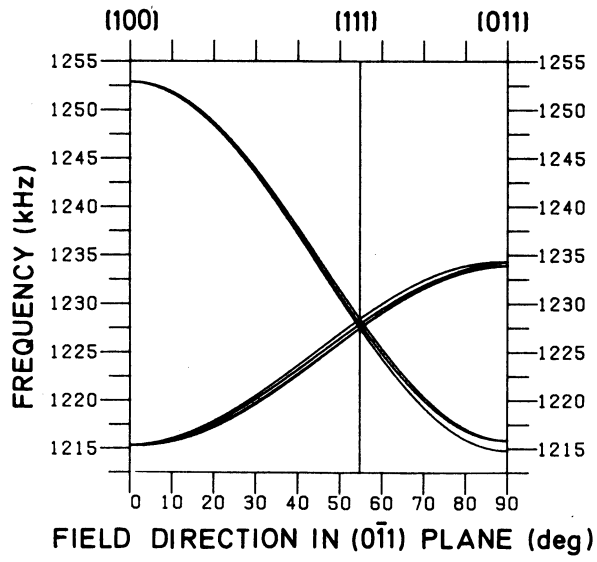

FIG. 9. Computer simulation of the angular dependence of the $2mm$ tensor; we assumed that it had the lower mirror class symmetry. $\frac{1}{2}A_{\text{eff}}$ is plotted.

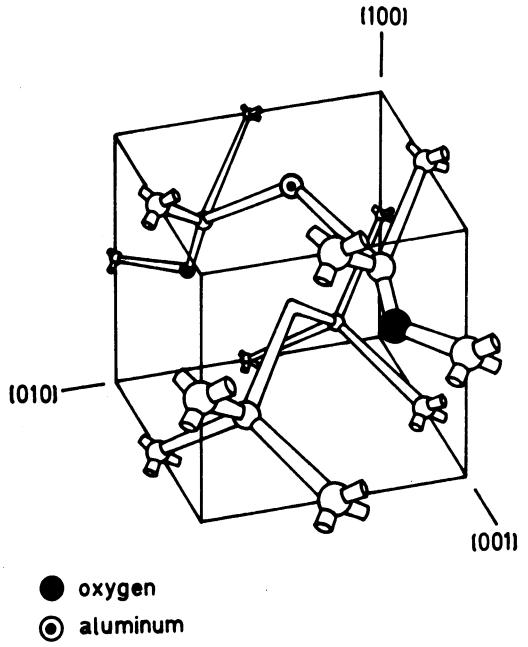

FIG. 10. Structural model for the Si:Al-NL10-1 center. The aluminum atom is shown on tetrahedral interstitial position; however the normal substitutional site could not be excluded by Gregorkiewicz *et al.*[15] The defect is shown in orientation *ad*.

center, is discarded also for the Si-NL10 defect. In the OSB model the double-donor character originates from a divalent silicon atom with two dangling-bond electrons which give the double donor action. A calculation predicted that the hyperfine interaction of the defect electron with this central silicon atom should be as high as 80 MHz.[30] In such case the ENDOR experiment should produce a prominent $2mm$ point-group symmetry class hyperfine tensor. As discussed before no prominent hyperfine-interaction tensor was observed, with the biggest tensor having the isotropic hyperfine interaction of only 2.5 MHz.

The current ^{29}Si-ENDOR data are in agreement with the new model as was proposed for the Si-NL10 center[15] and which is shown in Fig. 10. At first inspection of the results the "strong" $2mm$ silicon hyperfine tensor appears to be somewhat strange. A $2mm$ silicon hyperfine tensor originates from a silicon atom on the twofold axis. This means, without any distortions taken into account, that the position closest to the center of the defect is either (4,0,0) or (−4,0,0) [note that there is no silicon atom on (0,0,0)—see Fig. 10]. In view of the isotropic character of the defect wave function it seems at least suspicious that silicon atoms at next-nearest positions to the vacancy have weaker interactions than the atoms on the twofold axis. There are, however, two possibilities to explain the existence of this strong $2mm$ tensor. First, as proposed by Gregorkiewicz *et al.*,[15] similar structures as depicted in Fig. 10 can be produced with the aluminum nucleus replaced by a silicon nucleus. The localization found on the aluminum nucleus[15] is indeed comparable to the localization on the "$2mm$" silicon atom supporting such explanation. Secondly, as discussed in the previous section, it is also possible that the $2mm$ hyperfine tensor is not really of $2mm$, but rather of the mirror class. In that situation the silicon nucleus could be situated anywhere on the mirror plane. A position next to the vacancy would then be allowed.

V. CONCLUSIONS

The field-stepped ENDOR measurements indicate that the EPR spectrum of the Si-NL10 center is composed out of a few very similar EPR spectra with slightly different g values. The resolution of the EPR technique is not able to separate the different species which can only be achieved in the field-stepped ENDOR technique. The results are in agreement with the earlier oxygen and aluminum field-stepped ENDOR measurements. The three $2mm$ (T class) tensors are most probably originating from three different species; for two of them this conclusion was found experimentally, the intensity of the third prohibited its analysis with FSt ENDOR. In view of the above the g shifting of the spectrum Si-NL10–Si-NL13 and further to Si-NL17 can easily be explained as a varying concentration of different species can result in a semicontinuous g shifting process.

The Si-NL10 center has all characteristics of a shallow center, i.e., the reduced g values fall inside the area of shallow centers, the LCAO analysis of the silicon hyperfine tensors gives a/b and β^2/α^2 ratios typical for shallow centers, and the total localization of the defect electron which is traced in the experiment is very low [Table IV(c)]. The wave function of the defect can be described within the effective-mass theory. The wave function is constructed from a linear combination of Bloch functions located at the six conduction-band minima. It is concluded both from the $\langle 100 \rangle$-axial character of the hyperfine tensors and from the presence of a "big" $2mm$ class tensor, that the ground-state symmetry is of the A_1 type without symmetry-forbidden mirror planes.

The Si-NL10 center is created in concentrations up to those of the thermal donors concentration as determined from room-temperature resistivity measurements. Despite that, no infrared spectrum can be attributed to the Si-NL10 center. Therefore, in the model by Gregorkiewicz *et al.*[15] the Si-NL10 is related to the same thermal donor as Si-NL8 but in another charge state (or excited state). Indeed, there are several similarities between the Si-NL8 and Si-NL10 centers which support this idea.

(1) Both spectra are created by thermal annealing of oxygen-rich silicon at ~450 °C, regardless of the dopant.

(2) Both defects incorporate oxygen as impurity.

(3) Both defects develop a series of very similar species.

(4) Both EPR spectra exhibit a very uncommon g shift phenomenon.

(5) Both defects grow most probably by addition of oxygen atoms in the [011] direction.

(6) Both spectra originate from centers which fall in the category of shallow defects.

In addition to the above listed similarities the ENDOR

study presented here brings two more features which further link the two centers.

(7) Both spectra have an A_1 ground state.

(8) Both spectra have very similar ^{29}Si-ENDOR data, i.e., very similar spin function distribution with stronger delocalization for the Si-NL10 center.

ACKNOWLEDGMENT

This work has been supported by the Netherlands Foundation for Fundamental Research on Matter [Stichting voor Fundamenteel Onderzoek der Materie (FOM)].

---

*Also at Institute of Physics, Polish Academy of Sciences, PL-02-668 Warsaw, Poland.

[1]C. S. Fuller, J. A. Ditzenberger, N. B. Hannay, and E. Buehler, Phys. Rev. **96**, 833 (1954).

[2]C. S. Fuller and R. A. Logan, J. Appl. Phys. **28**, 1427 (1957).

[3]W. Kaiser, H. L. Frisch, and H. Reiss, Phys. Rev. **112**, 1546 (1958).

[4]A. Bourret, in *Proceedings of the 13th International Conference on Defects in Semiconductors, Coronado, 1984,* edited by L. C. Kimerling and J. M. Parsey, Jr. (The Metallurgical Society of the AIME, Warrendale, Pennsylvania, 1985), p. 129.

[5]D. Wruck and P. Gaworzewski, Phys. Status Solidi A **56**, 557 (1979).

[6]B. Pajot, H. Compain, J. Lerouille, and B. Clerjaud, Physica B+C **117&118B**, 110 (1983).

[7]S. H. Muller, M. Sprenger, E. G. Sieverts, and C. A. J. Ammerlaan, Solid State Commun. **25**, 987 (1978).

[8]S. H. Muller, E. G. Sieverts, and C. A. J. Ammerlaan, Inst. Phys. Conf. Ser. **46**, 297 (1979).

[9]K. M. Lee, J. M. Trombetta, and G. D. Watkins, in *Microscopic Identification of Electronic Defects in Semiconductors,* edited by N. M. Johnson, S. G. Bishop, and G. D. Watkins (Materials Research Society, Pennsylvania, 1985), Vol. 46, p. 263.

[10]T. Gregorkiewicz, D. A. van Wezep, H. H. P. Th. Bekman, and C. A. J. Ammerlaan, Phys. Rev. B **35**, 3810 (1987).

[11]H. H. P. Th. Bekman, T. Gregorkiewicz, and C. A. J. Ammerlaan, J. Appl. Phys. **62**, 4404 (1987).

[12]T. Gregorkiewicz, D. A. van Wezep, H. H. P. Th. Bekman, and C. A. J. Ammerlaan, Phys. Rev. Lett. **59**, 1702 (1987).

[13]J. Michel, J. R. Niklas, and J.-M. Spaeth, in *Defects in Electronic Materials,* edited by M. Stavola, S. J. Pearton, and G. Davies (Materials Research Society, Pennsylvania, 1987), Vol. 104, p. 185.

[14]J. Michel, J. R. Niklas, J.-M. Spaeth, and C. Weinert, Phys. Rev. Lett. **57**, 611 (1986).

[15]T. Gregorkiewicz, H. H. P. Th. Bekman, and C. A. J. Ammerlaan, Phys. Rev. B **38**, 3998 (1988).

[16]M. Sprenger, S. H. Muller, E. G. Sieverts, and C. A. J. Ammerlaan, Phys. Rev. B **35**, 1566 (1987).

[17]J. R. Morton and K. F. Preston, J. Magn. Reson. **30**, 577 (1978).

[18]E. G. Sieverts and S. H. Muller, Phys. Status Solidi B **110**, K89 (1982).

[19]E. G. Sieverts, S. H. Muller, and C. A. J. Ammerlaan, Phys. Rev. B **18**, 6834 (1978).

[20]L. M. Roth, Phys. Rev. **118**, 1534 (1960).

[21]L. Liu, Phys. Rev. Lett. **6**, 683 (1961).

[22]L. Liu, Phys. Rev. **126**, 1317 (1962).

[23]T. G. Castner and H. S. Tan, Solid State Commun. **26**, 389 (1978).

[24]Y. H. Lee and J. W. Corbett, Phys. Rev. B **8**, 2810 (1973).

[25]E. G. Sieverts, Phys. Status Solidi B **120**, 11 (1983).

[26]W. Kohn, in *Solid State Physics,* edited by F. Seitz and D. Turnbull (Academic, New York, 1957), Vol. 5, p. 257.

[27]W. Kohn and J. M. Luttinger, Phys. Rev. **98**, 915 (1955).

[28]M. Stavola and K. M. Lee, in *Oxygen, Carbon, Hydrogen and Nitrogen in Crystalline Silicon,* edited by J. C. Mikkelsen, Jr., S. J. Pearton, J. W. Corbett, and S. J. Pennycook (Materials Research Society, Pennsylvania, 1986), Vol. 59, p. 95.

[29]A. Ourmazd, W. Schröter, and A. Bourret, J. Appl. Phys. **56**, 1670 (1984).

[30]J. Robertson and A. Ourmazd, Appl. Phys. Lett. **46**, 559 (1985).

[31]E. B. Hale and R. L. Mieher, Phys. Rev. **184**, 739 (1969).